Wind Turbine Design Optimization for Hydrogen Production

Preprint

Jared J. Thomas,[1] Cameron Irmas,[1] Genevieve Starke,[1] Zachary Tully,[2] Elenya Grant,[1] Nicholas Riccobono,[1] Kazunori Nagasawa,[1] and Christopher J. Bay[1]

1 National Renewable Energy Laboratory
2 Advanced Energy Systems, Colorado School of Mines

Presented at the 8th Hybrid Power Plants & Systems Workshop
Azores, Portugal
May 14–15, 2024

NREL is a national laboratory of the U.S. Department of Energy
Office of Energy Efficiency & Renewable Energy
Operated by the Alliance for Sustainable Energy, LLC

This report is available at no cost from the National Renewable Energy Laboratory (NREL) at www.nrel.gov/publications.

Contract No. DE-AC36-08GO28308

Conference Paper
NREL/CP-5000-89660
July 2024

Wind Turbine Design Optimization for Hydrogen Production

Preprint

Jared J. Thomas,[1] Cameron Irmas,[1] Genevieve Starke,[1] Zachary Tully,[2] Elenya Grant,[1] Nicholas Riccobono,[1] Kazunori Nagasawa,[1] and Christopher J. Bay[1]

1 National Renewable Energy Laboratory
2 Advanced Energy Systems, Colorado School of Mines

Suggested Citation
Thomas, Jared J., Cameron Irmas, Genevieve Starke, Zachary Tully, Elenya Grant, Nicholas Riccobono, Kazunori Nagasawa, Christopher J. Bay. 2024. *Wind Turbine Design Optimization for Hydrogen Production: Preprint*. Golden, CO: National Renewable Energy Laboratory. NREL/CP-5000-89660. https://www.nrel.gov/docs/fy24osti/89660.pdf.

NREL is a national laboratory of the U.S. Department of Energy
Office of Energy Efficiency & Renewable Energy
Operated by the Alliance for Sustainable Energy, LLC

This report is available at no cost from the National Renewable Energy Laboratory (NREL) at www.nrel.gov/publications.

Contract No. DE-AC36-08GO28308

Conference Paper
NREL/CP-5000-89660
July 2024

National Renewable Energy Laboratory
15013 Denver West Parkway
Golden, CO 80401
303-275-3000 • www.nrel.gov

NOTICE

This work was authored in part by the National Renewable Energy Laboratory, operated by Alliance for Sustainable Energy, LLC, for the U.S. Department of Energy (DOE) under Contract No. DE-AC36-08GO28308. Funding provided by the U.S. Department of Energy Office of Energy Efficiency and Renewable Energy Wind Energy Technologies Office. The views expressed herein do not necessarily represent the views of the DOE or the U.S. Government. The U.S. Government retains and the publisher, by accepting the article for publication, acknowledges that the U.S. Government retains a nonexclusive, paid-up, irrevocable, worldwide license to publish or reproduce the published form of this work, or allow others to do so, for U.S. Government purposes.

This report is available at no cost from the National Renewable Energy Laboratory (NREL) at www.nrel.gov/publications.

U.S. Department of Energy (DOE) reports produced after 1991 and a growing number of pre-1991 documents are available free via www.OSTI.gov.

Cover Photos by Dennis Schroeder: (clockwise, left to right) NREL 51934, NREL 45897, NREL 42160, NREL 45891, NREL 48097, NREL 46526.

NREL prints on paper that contains recycled content.

WIND TURBINE DESIGN OPTIMIZATION FOR HYDROGEN PRODUCTION

*Jared J. Thomas[1], Cameron Irmas[1], Genevieve Starke[1], Zachary Tully[2], Elenya Grant[1], Nicholas Riccobono[1], Kazunori Nagasawa[1], Christopher J. Bay[1]**

[1]*National Renewable Energy Laboratory, Golden, CO, USA*
[2]*Advanced Energy Systems, Colorado School of Mines, Golden, CO, USA*
[*]*christopher.bay@nrel.gov*

Keywords: WIND TURBINE DESIGN, HYDROGEN, OPTIMIZATION

Abstract

To help meet the need for inexpensive green hydrogen, a framework for wind turbine design optimization specifically for hydrogen production has been developed. This framework optimizes wind turbines by minimizing a levelized cost of hydrogen (LCOH) objective. Preliminary case study results show a 1.53% decrease in LCOH when compared to an LCOE optimized turbine using our framework. The decrease in LCOH from the baseline reference turbine to the LCOH optimized turbine was 12.7%. The decrease in LCOE from the baseline reference turbine to the LCOE optimized turbine was 12.35%. The LCOH optimized turbine has a larger rotor compared to the baseline and LCOE optimized turbines, where the increased turbine cost is offset by increased hydrogen production. This case study focuses on a single wind turbine-electrolyzer system, demonstrating that significant cost savings can be achieved by using new optimization objectives. Further cost savings may be had with plant-level optimizations and by including other technologies such as solar panels and battery storage.

1 Introduction

As pressure builds to limit climate change through decarbonization, hydrogen is of particular interest for decarbonizing areas that are carbon heavy, such as personal transportation, freight logistics, and industrial processes [1]. Different types of hydrogen production methods have been classified based on their relative carbon footprints: grey/brown hydrogen are made using natural gas/coal respectively and have the largest carbon footprint; blue hydrogen is produced from fossil fuels, but emissions are offset with carbon capture and storage technologies; green hydrogen is produced using zero-carbon electricity sources such as wind and solar power [2].

As such, green hydrogen is an attractive candidate to help achieve the U.S. and other governments' renewable energy and emission reduction goals [3, 4]. However, green hydrogen is significantly more expensive than hydrogen produced from, or as a byproduct of, fossil fuels [5]. With wind being an abundant source of renewable energy, it is important to investigate ways in which the cost of hydrogen produced using wind energy can be reduced.

Wind turbines are often optimized to minimize the cost of energy [6]. The power produced from these turbines is variable, as the wind is an intermittent resource, but also because wind turbines have been optimized for maximum total, long-term energy production with no consideration of minimizing short-term variability. However, in a scenario in which the wind turbines are directly connected to the electrolysis system, there are nuances in the production of hydrogen that may make a turbine optimized for the cost of energy suboptimal. For instance, electrolyzers can possibly degrade when turned on and off [7] or when are operated with a variable power signal [8]. Thus it would be good to account for the impacts of the variable and intermittent wind energy on the electrolyzer cost and operation. If electrolyzers degrade faster the stacks need to be replaced more frequently, driving up the cost of hydrogen. For this reason it may be best to have steady power, and a guaranteed minimum power, when producing hydrogen. An optimal turbine design may therefore be designed for more consistent power rather than for the lowest cost of energy.

Optimizing a wind turbine for minimum cost of energy leads to designs that maximize energy production while minimizing the wind turbine manufacturing cost, typically resulting in a balanced rotor size between cost and energy capture. Such an approach may increase the cost of hydrogen even if the overall cost of energy is lower, benefiting from capturing peaks in energy production and limiting energy capture in lower wind speeds. This results in a more variable power production from the wind turbine, which in turn can cause fluctuations in hydrogen production. In [5], design sweeps of rotor diameter and wind turbine power rating for both the levelized cost of energy (LCOE) and the levelized cost of hydrogen (LCOH) were performed. They found only a small difference between the designs for LCOE and LCOH. However, they did not include a redesign of the blades. When the rotor diameter is increased, the wind turbine performance changes and design variables such as twist and chord may no longer be optimal.

With this in mind, the authors have devised the necessary modeling and optimization framework to perform wind turbine design for hydrogen production. This framework includes a new open-source electrolyzer simulator to model hydrogen production, degradation, and LCOH based on experimental

This report is available at no cost from the National Renewable Energy Laboratory at www.nrel.gov/publications.

data and industry input, which is coupled with an open-source wind turbine design tool.

As an initial case study, an onshore location near the Gulf of Mexico region was chosen based on customer feedback and interest in potential wind-hydrogen systems. A baseline turbine, the International Energy Agency (IEA) 3.4 MW reference turbine [9], was used as a starting point. The optimizations were completed in sequential steps, first with a tower redesign to better match onshore transportation limits for tower sections. Next, the tower and blades were optimized by adjusting the blade chord, twist, spar cap thickness, tower height, and tower section thickness. The last step optimized the drivetrain for the redesigned rotor, adjusting numerous geometrical parameters. These optimizations were run for two different objectives: 1) minimize LCOE, and 2) minimize LCOH.

In the following sections we will provide an overview of our methods, the optimization framework, and the results from an initial case study, before presenting conclusions and future work.

2 Methods

We used the Wind-plant Integrated System Design and Engineering Model (WISDEM) [10] to model the wind turbine. WISDEM is written in Python using OpenMDAO [11], a tool developed by NASA to facilitate multidisciplinary analysis and optimization. WISDEM includes performance and cost models for each major wind turbine component.

We also extended WISDEM to include hydrogen production performance and costs from Electrolyzer [12], a new tool in development at National Renewable Energy Laboratory (NREL) for modeling the performance and costs of electrolysis systems. Although WISDEM typically works with statistical wind turbine performance, we included a specific wind profile so we could more accurately capture the hourly performance of the electrolyzer. Including hourly performance is critical in order to capture the degradation of the electrolyzer due to on/off cycles, variable power during operation, and operating below rated power.

Fig. 1 shows the turbine design process as an eXtended Design Structure Matrix diagram. The driver of the optimization is SNOPT, a sparse nonlinear optimization algorithm [13]. The optimizer takes in initial conditions and begins iterating, passing design variables for the turbine to WISDEM. WISDEM optimizes the tower, rotor blades, and drivetrain of the wind turbine in a 3-part process that is described in Section 2.4. WISDEM then produces a turbine design that we can use to predict the power produced given a wind profile, in addition to the cost of the turbine. With this information, LCOE is determined and passed along with power produced to the Electrolzyer software, which produces an LCOH for the given turbine design. Details of the models, design variables, constraints, and objectives are given below.

2.1 Wind turbine model

We used the IEA 3.4 MW reference land-based wind turbine [9] as the baseline design. This decision was informed by our industry partners as well as available reference turbines. An overview of the IEA 3.4 MW turbine is given in Table 1.

Table 1 Overview of the IEA 3.4 MW reference turbine [9]

Characteristic	Value
Rotor diameter (m)	130
Hub height (m)	110
Nameplate power (MW)	3.37
Specific power (W/m^2)	254
Cut-in wind speed (m/s)	4
Cut-out wind speed (m/s)	25

The wind turbine costs and physics were modeled using WISDEM [10], a collection of modules that enable wind turbine modeling and design optimization. The primary WISDEM modules leveraged in this work were RotorSE, TowerSE, DrivetrainSE, and LandBOSSE.

2.1.1 Physics Modeling: The wind turbine rotor physics were modeled using RotorSE, which is a combination of steady-state models. The aerodynamics are handled by CCBlade (a blade element momentum model), the cross-sectional elastic properties of the blades are modeled by PreComp, and the deformations are estimated using a Timoshenko beam solver, Frame3DD. Strains, deflections, load estimates, and annual energy are also calculated in RotorSE.

The wind turbine tower physics were modeled with TowerSE. TowerSE includes engineering models for global buckling, shell buckling, and stress. Cylindrical tower sections are used to estimate the axial and sheer stress. Von Mises stress is obtained by combining the axial and stress estimates with hoop stress. TowerSE also estimates fatigue.

The drivetrain forces, moments, efficiency, and mass properties in WISDEM are modeled using DrivetrainSE. DrivetrainSE directly models, and can estimate the size of, the major components of the drive train based on the rotor properties and aerodynamic loads. DrivetrainSE relies heavily on Frame3DD for analysis. For more information on these modules, see [10].

2.1.2 Cost and Financial Modeling: The cost modeling in WISDEM begins with RotorSE, which provides a bottom-up cost model for the wind turbine blades. The turbine capital costs, transportation costs, and balance of system costs (including installation) are modeled using LandBOSSE, a tool specifically for estimating land-based utility scale wind project costs. The costs scale based on the output from the other WISDEM modules, including hub height, blade mass, nacelle mass, tower mass, and wind turbine rating. In WISDEM, LCOE is estimated based on the total costs and an estimated annual energy production for the given turbine design.

This report is available at no cost from the National Renewable Energy Laboratory at www.nrel.gov/publications.

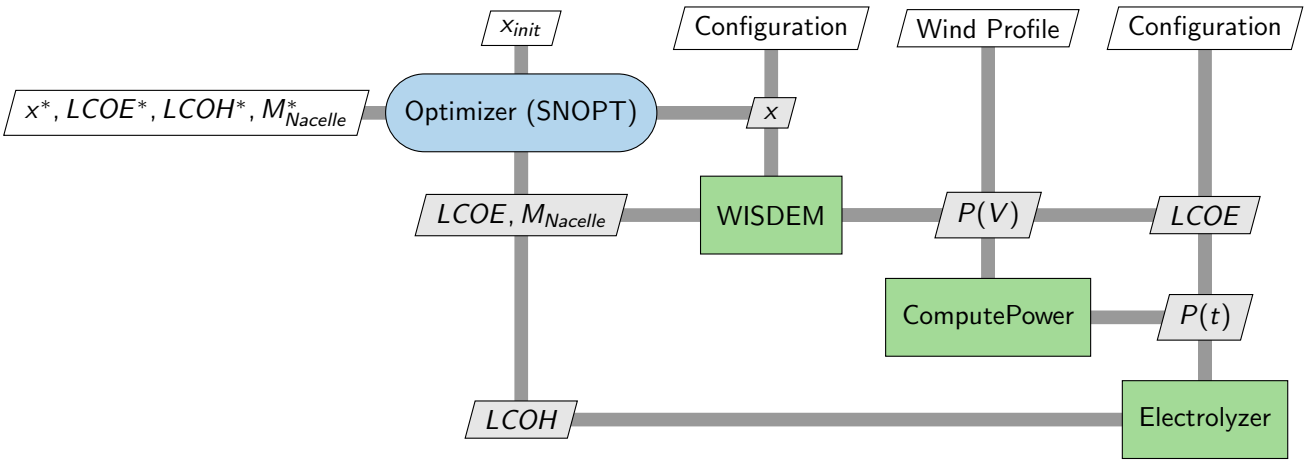

Fig. 1 An eXtended Design Structure Matrix diagram showing the wind turbine design optimization problem structure. Note that the WISDEM block is itself a group of models and also returns more information than shown, including the blade tip deflection, blade strains, tower stress, and tower buckling values for use in optimization constraints.

2.2 Electrolyzer model

2.2.1 Electrolyzer Physics Model: The Electrolyzer [12] model is an open-source model that starts at the cell level, e.g. electrochemistry, of the electrolyzer, and builds the stacks out of these cell blocks, then the electrolysis plant out of stacks. This study uses a polymer electrolyte membrane electrolyzer type, which is what the following equations describe. The power consumed by a single stack, denoted P_{dc}, is calculated as the product of the stack current (I), stack voltage (V), and the number of cells in the stack (n_{cells}),

$$P_{\text{stack}} = I \cdot V_{\text{cell}} \cdot n_{\text{cells}}$$

The stack current is found using a polarization curve that is fitted to the model behavior at the beginning of the simulation using a fourth-order polynomial relationship. Then the current is determined from the polarization curve at each time step using the input power to the electrolyzer stack and the stack temperature.

The cell voltage, in turn, is calculated in multiple steps. The reversible cell voltage is calculated using the Gibbs free energy of reaction (ΔG^0_R), the number of moles of electrons transferred in the reaction (n), and Faraday's constant (F),

$$E_{rev,0} = \frac{\Delta G^0_R}{nF}$$

The open circuit voltage (E_{cell}) is calculated using the Nernst equation, which considers the temperature (T), the atmospheric pressure (P_{atmo}), and the vapor pressure of water at the given temperature ($p_{H_2O,sat}$),

$$E_{\text{cell}} = E_{\text{rev},0} + \frac{RT}{nF} \ln\left(\frac{p_{\text{a}} - p_{\text{H}_2\text{O,sat}}}{P_{\text{atm}}} \sqrt{\frac{p_{\text{c}} - p_{\text{H}_2\text{O,sat}}}{P_{\text{atm}}}}\right)$$

The final cell voltage is then calculated using the open circuit voltage and overpotentials. The activation overpotential (V_{act}) is calculated using the Butler-Volmer equation, and considers the charge transfer coefficient (α), the exchange current density (i_0), and the temperature at the anode and cathode (T_a and T_c) [14]. The Ohmic overpotential (V_{ohm}) is the voltage loss due to resistance in the electrolyte and electrode material, and considers the properties of the electrolyte and the electronic and ionic resistance ($R_{\text{ohm,elec}}$ and $R_{\text{ohm,ionic}}$) [15]. The concentration overpotential (V_{conc})—the voltage loss due to concentration changes in the reactants and products at the electrodes—is not yet implemented in Electrolyzer. The full voltage calculation is represented as

$$\begin{aligned}
V_{\text{cell}} &= E_{\text{cell}} + V_{\text{act,a}} + V_{\text{act,c}} + V_{\text{ohm}} + V_{\text{conc}} \\
V_{\text{act,a}} &= \frac{RT_a}{\alpha_a F} \sinh^{-1}\left(\frac{i}{2i_{0,a}}\right) \\
V_{\text{act,c}} &= \frac{RT_c}{\alpha_c F} \sinh^{-1}\left(\frac{i}{2i_{0,c}}\right) \\
V_{\text{ohm}} &= i \cdot (R_{\text{ohm,elec}} + R_{\text{ohm,ionic}}) \\
V_{\text{conc}} &= 0
\end{aligned}$$

The hydrogen mass flow rate of the stack is found using the following expression,

$$mfr = \eta_F \; I \; \frac{M}{nF}(1 - \eta_{dryer}) n_{cells} \times 10^{-3}, \qquad (1)$$

where mfr is the mass flow rate of hydrogen produced from a stack in kilograms per second, η_F is Faraday's efficiency, defined as in [16], I is the stack current, M the molecular weight in grams/mol, $M = 2.016$, and $\eta_{dryer} = 0.065$ is the efficiency loss of drying hydrogen.

The scaling algorithm uses this definition of stack power to appropriately size electrolyzer systems based on initial parameters of system size (P_{sys}), maximum current (I_0), cell area (A_0),

This report is available at no cost from the National Renewable Energy Laboratory at www.nrel.gov/publications.

and number of cells ($n_{\text{cells,0}}$). This scaling is done so that the electrolyzer system can be smoothly scaled, which is useful for optimizations. First, we determine the number of stacks,

$$p_{\text{stack,0}} = P_{\text{stack}}(I_0, A_0, n_{\text{cells,0}})$$
$$n_{\text{stacks}} = \left\lfloor \frac{P_{\text{sys}}}{p_{\text{stack,0}}} \right\rceil$$

We then we define the desired stack power rating and desired maximum current density,

$$P_{\text{desired}} = \frac{P_{\text{sys}}}{n_{\text{stacks}}}$$
$$J_{\text{desired}} = \frac{I_0}{A_0}$$

Next, we determine the number of cells (n_{cells}) by iteratively incrementing or decrementing until the desired stack rating (P_{desired}) is approximately reached. One iteration is as follows:

$$n_{\text{cells}} = n_{\text{cells}} \pm 1$$
$$p_{\text{stack}} = P_{\text{stack}}(I_0, A_0, n_{\text{cells}})$$

Finally, we adjust to meet the desired stack rating by solving the nonlinear equations for current (I) and cell area (A),

$$\begin{cases} P_{\text{stack}}(I, A, n_{\text{cells}}) - P_{\text{desired}} & = 0 \\ \frac{I}{A} - J_{\text{desired}} & = 0 \end{cases}$$

The Electrolyzer model also approximates degradation of the electrolyzer using three quantities: 1) the total runtime of the electrolyzer, 2) the variability in the power input signal, and 3) the number of start-up/shutdown cycles that occur when the input power becomes too low. The effects of these three operations are aggregated into a voltage penalty that requires the electrolyzer to use more power to produce the same amount of hydrogen (H_2) over time. To help mitigate these degradation effects, a control strategy is used to distribute the power among the electrolyzer stacks. The specific strategy used is called "BaselineDeg", which is the default control strategy for the Electrolyzer model. The details of how the Electrolyzer model performs the degradation calculation as well as the control strategy are given in [17].

2.2.2 Electrolyzer Cost Model: The electrolyzer costs were modeled as a combination of capital expenditures (CapEx), operation and maintenance expenditures (OpEx), stack replacement costs, and feedstock costs. The CapEx were modeled after the technique used by [18] in Table 2.1, with the equations repeated here for completeness. The CapEx is calculated as:

$$P_{elec} RC_{elec} \left(1 + IF \cdot OS\right) \left(\frac{P_{elec}}{RP_{elec}}\right)^{SF_{elec}}$$

where P_{elec} is the capacity rating of the electrolyzer, RC_{elec} is the reference cost of the electrolyzer system for costscaling purposes, IF is the installation factor that changes depending on onshore or offshore configurations, OS is a boolean value to indicate onshore or offshore, RP_{elec} is the reference plant size for cost scaling purposes, and SF_{elec} is a scaling factor that represents a learning rate associated with economies of scale defined as $SF_{elec} = log_2(1 - LR)$ where LR is the learning rate. For further details on the CapEx calculation, see [18]. Two CapEx sources were calculated, one for the electrolyzer stack and one for the balance of plant (BOP) to cover associated other equipment. Values used for this optimization are summarized in the Table 2.

Table 2 CapEx inputs used in the turbine design optimization

Input	Value	Input	Value
RC_{elec} (\$/kW)	695	IF	0.33
RC_{bop} (\$/kW)	747	OS	0
RP_{elec} (kW)	2000	LR	0.13
RP_{bop} (kW)	200		

The OpEx costs were calculated as a combination of variable (VOM) and fixed (FOM) operating costs,

$$P_{elec,plant} \left(CF \cdot VOM + FOM\right)$$

where $P_{elec,plant}$ is the total electrolyzer plant power rating and CF is the power usage capacity factor of the electrolyzer plant calculated as $CF = P_{consumed}/P_{rated,consumed}$. The OpEx inputs were taken from Table S25 of the supplementary materials of [19] and are $VOM = 0.0013$ \$/kWh and $FOM = 12.8$ \$/kW-year.

The stack replacement cost was modeled as a fixed percent (15%) of the uninstalled CapEx cost of the electrolyzer. Based on the approximated stack degradation calculated as described above, a replacement schedule for the electrolyzer stacks was determined when an increase in cell voltages reached 0.7212 V compared to their initial voltage. The cost of the replacement was added in the year that it occurred.

Lastly, the feedstock costs included in the design optimization were just the water costs, as the system was configured to be off-grid. The water used was calculated as a linear relationship to the H_2 produced, with the rate being defined by the user. The value used for the optimizations was 10 kgH_2O/kgH_2, with the cost of water as 0.0008 \$/kgH_2O.

2.3 Metrics

The LCOE is defined as the unit cost of energy that would exactly balance the costs of the energy generation if discounted to the base year [20][21].

$$LCOE = \frac{C_E}{E}, \tag{2}$$

where C_E is the total costs of the electricity generation over the life of the plant, and E is the total energy produced over the life

This report is available at no cost from the National Renewable Energy Laboratory at www.nrel.gov/publications.

of the plant. We defined the LCOH similarly as [18]

$$LCOH = \frac{\sum_{Y=0}^{L_P} \frac{[LCOE][E_Y]+C_{H_2,Y}}{(1+r)^Y}}{\sum_{Y=0}^{L_P} \frac{M_{H_2,Y}}{(1+r)^Y}}, \quad (3)$$

where E_Y is the energy used in year Y, $C_{H_2,Y}$ is the total capital and operational costs of the hydrogen generation in year Y excluding the cost of energy, $M_{H_2,Y}$ is the mass of hydrogen produced in year Y, r is the discount rate, and L_P is life of the plant in years.

Equation (3) shows us that we can reduce the LCOH in four basic ways: (1) reduce the LCOE, (2) use less energy (reduce E_Y), (3) lower the other costs of hydrogen (reduce $C_{H_2,Y}$), or (4) generate more hydrogen at the same cost (increase $M_{H_2,Y}$). We can simultaneously address all of these factors of LCOH by including the electrolyzer physics and cost considerations in the wind turbine design loop.

2.4 Optimization

Rather than run a single optimization with all the design variables at once, we opted for a three-part optimization approach. First, because the IEA 3.4 MW wind turbine tower is too large for transport on land, we redesigned the wind turbine tower to get a tower that was suitable for overland transportation. Second, we swept the electrolyzer rating and turbine rotor diameter and ran a combined aero-structural optimization of the blades and tower at each combination of electrolyzer rating and wind turbine rotor diameter. Finally we optimized the drivetrain system to reduce mass.

For the first step, the tower redesign, we used the tower thickness and diameter at eleven locations along the tower as the design variables. We constrained the tower diameter (d) to be less than or equal to 4.3 m and greater than or equal to 3.5 m. We constrained the tower thickness (t) to be between 0.003 m and 0.2 m. We additionally included constraints on the maximum von Mises stress (checks against yield limit) (C_σ), global buckling (b_g), shell buckling (b_s), tower slope, and the first natural frequency (λ_i) of the tower. The complete objective function we used for the tower optimization was

$$\begin{aligned}
\text{minimize} \quad & LCOE(t, d) \\
\text{tower subject to} \quad & 0.004 \text{ m} \leq t_k \leq 0.2 \text{ m}, \quad k = 1...11 \\
& 3.5 \text{ m} \leq d_k \leq 4.3 \text{ m}, \quad k = 1...11 \\
& b_{g,i} < 1, i = 1...8 \\
& b_{s,i} < 1, i = 1...8 \\
& C_{\sigma,i} < 1, i = 1...8 \\
& 0.13 \leq \lambda_{1,i} \leq 0.4, i = 1...8,
\end{aligned} \quad (4)$$

For the second step, we used the electrolyzer and turbine diameter as swept variables to give us an idea of the shape of the design space. We used both LCOE and LCOH as our objective functions so we could compare the resulting turbine designs found using each objective. Although the optimal relative size of wind energy and electrolysis systems is uncertain [5], we chose to keep the electrolyzer rating and the wind turbine rotor diameter fixed during optimization. The design variables we chose were blade twist (θ) and chord (c) at 8 locations along the blade, spar cap thickness (T) at 8 points along the blade (pressure side and suction side spar cap thickness were required to be the same), and the thickness of the layers in each section of the wind turbine tower (t). The blade design constraints were bounds on the change in twist, bounds on the change in chord, bounds on change in the spar cap thickness, stall margin (M_s), maximum chord, spar cap strains at 7 locations along the blade for both the pressure side (L) and suction side (U), tip deflection ratio (r_d), and the ratio between the recommended blade root circle diameter (d_r) and the chord at the blade root (c_r) . Tower design constraints were bounds on the tower layer thickness (t), von Mises stress constraint (checks against yield limit) (C_σ), global buckling (b_g), shell buckling (b_s), and the frequency ratio between the blade fundamental frequency and blade passing (3P) frequency at rated conditions (f).

The objective function was defined, for both the LCOE and LCOH objectives as

$$\begin{aligned}
\text{minimize} \quad & Objective(T_i, c_j, t_k, \theta_l) \\
\text{rotor subject to} \quad & 100 \text{ m} \leq D_i \leq 200 \text{ m} \\
& 0.8c_o \geq c_i \leq 2.0c_o, i = 1...8 \\
& \theta_i \geq \theta_{i,o} - 0.0872 \text{ rad}, i = 1...8 \\
& \theta_i \leq \theta_{i,o} + 0.0872 \text{ rad}, i = 1...8 \\
& 0.2T_o \geq T_i \leq 2.0T_o, i = 1...8 \\
& L_i \leq 0.0035, i = 1...7 \\
& U_i \leq 0.0035, i = 1...7 \\
& M_{s,i} \leq 0.05233 \text{ rad}, i = 1...8 \\
& r_{d,i} \leq 1.1 \\
& d_r/c_r \leq 1.0 \\
\text{tower subject to} \quad & 0.004 \leq t \leq 0.2 \\
& C_{\sigma,i} < 1, i = 1...8 \\
& b_{g,i} < 1, i = 1...8 \\
& b_{s,i} < 1, i = 1...8 \\
& f/3P < 0.9 \vee f/3P > 1.1
\end{aligned} \quad (5)$$

where ($i = 1...8$) indicates that the related variable or constraint was applied at 8 different locations along the blade or tower.

The third, and final step, was optimizing the drivetrain while holding the rest of the turbine design constant. For this step, we used the nacelle mass ($M_{nacelle}$) as the objective with the design variables being the shaft length from main bearing one to main bearing two (L_{12}), shaft length from the hub flange to main bearing one (L_{h1}), high-speed shaft length (L_{hss}), hub diameter (D), low-speed shaft length (d_{lss}), low-speed shaft wall thickness (t_{lss}), high-speed shaft diameter (d_{hss}), high-speed shaft wall thickness (t_{hss}), bedplate web thickness (t_{web}),

This report is available at no cost from the National Renewable Energy Laboratory at www.nrel.gov/publications.

bedplate flange thickness (t_{flange}), and bedplate flange width (w_{flange}). We placed bounds on all design variables. The other constraints for the drivetrain optimization were the low-speed shaft Von Mises stress ($\sigma_{v,lss}$), high-speed shaft Von Mises stress ($\sigma_{v,hss}$), bedplate Von Mises stress (($\sigma_{v,bp}$), main bearing one deflection angle ($\delta\theta_{b1}$), main bearing two deflection angle ($\delta\theta_{b2}$), hub diameter (d_h), margin for drivetrain length and desired overhang distance (M_l), margin for drivetrain height and desired hub height (M_h), shaft deflection (y_{sh}), shaft angle (θ_{sh}), stator angle (θ_{st}), and low speed shaft length (L_{lss}). The final optimization problem can be defined as

$$
\begin{aligned}
\text{minimize} \quad & M_{nacelle}(L_{12}, L_{h1}, L_{hss}, d_h, d_{lss}, t_{lss}, d_{hss}, t_{hss}, \\
& t_{web}, t_{flange}, w_{flange}) \\
\text{subject to} \quad & 0.1 \text{ m} \leq L_{12} \leq 1.0 \text{ m} \\
& 0.1 \text{ m} \leq L_{h1} \leq 2.0 \text{ m} \\
& 0.1 \text{ m} \leq L_{hss} \leq 1.5 \text{ m} \\
& 2.0 \text{ m} \leq d_h \leq 5.0 \text{ m} \\
& 0.3 \text{ m} \leq d_{lss} \leq 1.5 \text{ m} \\
& 4 \times 10^{-}3 \text{ m} \leq t_{lss} \leq 0.29 \text{ m} \\
& 0.2 \text{ m} \leq d_{hss} \leq 1.0 \text{ m} \\
& 0.004 \text{ m} \leq t_{hss} \leq 0.15 \text{ m} \\
& 0.004 \text{ m} \leq t_{web} \leq 0.5 \text{ m} \\
& 0.004 \text{ m} \leq t_{flange} \leq 0.5 \text{ m} \\
& 0.1 \text{ m} \leq w_{flange} \leq 1.0 \text{ m} \\
& \sigma_{v,lss} \leq 1.0, \quad \sigma_{v,hss} \leq 1.0, \quad \sigma_{v,bp} \leq 1.0 \\
& \delta\theta_{b1} \leq 0.008 \text{ rad}, \quad \delta\theta_{b2} \leq 0.008 \text{ rad} \\
& d_h \geq 0.0 \text{ m}, \quad M_l \geq 0.0, \quad M_h \geq 0.0 \\
& y_{sh} \leq 10^{-4} \text{ m}, \quad \theta_{sh} \leq 0.001 \text{ rad} \\
& \theta_{st} \leq 0.001 \text{ rad}, \quad L_{lss} \geq 0.1 \text{ m}
\end{aligned}
\tag{6}
$$

We used the sparse nonlinear optimization algorithm SNOPT to solve the optimization problem with a convergence tolerance of $1 \times 10^{-}3$. Gradients were computed using central finite differences to increase accuracy. The optimization was run with parallel derivative calculations on 64 cores using Dual Intel Xeon Gold Skylake 6154 (3.0 GHz, 18-core) processors using Eagle, the high performance super computer at the National Renewable Energy Laboratory.

3 Results and Discussion

The tower optimization resulted in a new tower design for the IEA 3.4 MW wind turbine with diameters less than 4.3 m, suitable for transport overland. The new tower design diameters were held constant during the second and third optimization steps. Designs were generated for minimizing LCOH and LCOE, with the LCOE results being generated for comparison. A site along the Gulf Coast of Mexico in Texas was used in the optimization. This area was identified through industry feedback and a wind resource profile was collected from the U.S. Wind Toolkit database [22]. Both cases showed reductions in cost from the IEA 3.4 MW reference wind turbine baseline design.

For the LCOE minimization, the optimizer drove the turbine to a larger rotor size of 150 m from the baseline of 130 m for a 12.35% reduction in LCOE, as shown in Fig. 2. This is not surprising for this location as the average wind speeds in the Gulf of Mexico are lower than most onshore locations in the United States that have seen significant wind energy development. The two main steps of the optimization are shown with the blue results capturing the tower and rotor design optimization, followed by the drivetrain optimization shown with the green dots.

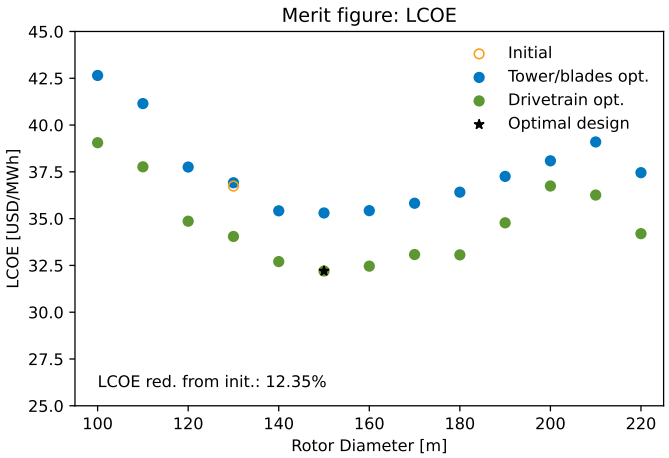

Fig. 2 Levelived cost of energy (LCOE) optimization results with different sizes of rotor diameter where the optimized turbine design gives a total LCOE reduction of 12.35% compared to the baseline turbine design.

As the rotor diameter continues to increase, LCOE begins to rise again as we would expect due to increasing CapEx with less energy production to offset the cost. As the design nears a rotor diameter of 200 m, we begin to see deviations in the cost trend, most likely due to the cost models not being applicable for such a large onshore wind turbine.

Fig. 3 shows the design results for the turbine when the optimization is minimizing LCOH. Here, the optimal rotor diameter is found to be even larger, at 170 m, giving a 12.7% reduction in LCOH from the baseline turbine, and an additional 1.53% in LCOH from the LCOE optimized turbine. Again, it can be seen as the rotor diameter approaches the 200 m mark, the optimization trend begins to diverge.

We hypothesize that the reduction in LCOH is largely coming from improved electrolyzer use. This improved up-time stems from the shifting of the wind turbine power curve to the left, shown in Fig. 4. As the rotor diameter increases, the "knee" of the power curve shifts to the left, towards lower wind speeds, reflecting a lowering of the rated wind speed for the designed turbine. In the Gulf Coast region, with the lower

This report is available at no cost from the National Renewable Energy Laboratory at www.nrel.gov/publications.

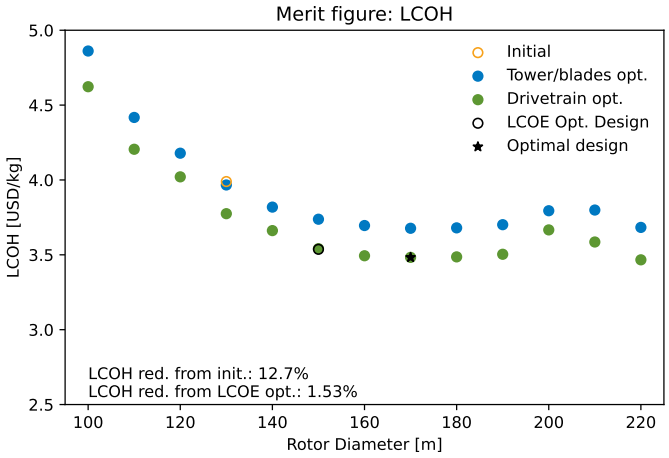

Fig. 3 Levelized cost of hydrogen (LCOH) optimization results with different sizes of rotor diameter where the optimized turbine design gives a total LCOH reduction of 12.7% compared to the baseline turbine design and an additional 1.53% reduction in LCOH from the LCOE optimized turbine.

average wind speeds, the authors believe this leads to producing rated power more of the time, thus increasing electrolyzer uptime and decreasing both low and no hydrogen production times. This increased production of hydrogen then offsets the increased cost of a larger turbine rotor. Additional analysis is needed to confirm this reasoning for the decrease in LCOH.

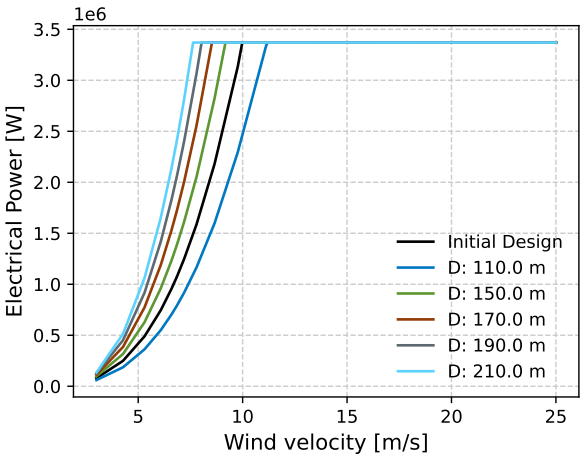

Fig. 4 Electrical power curves of the LCOH optimized turbine designs as rotor diameter (D) increases, showing a shift of the power curve to the left allowing turbines to hit rated power at lower wind speeds. The initial design has a rotor diameter of 130 m.

In the results in Fig. 4, the electrolyzer rating was held constant at a 1:1 ratio to the wind turbine power rating. Fig. 5 shows the LCOH for a wind-to-H_2 system where both the rotor diameter and the electrolyzer rating are varied. In this system, it appears that a 1:1 ratio of approximately 3.4 MW:3.4 MW does result in the lowest LCOH, with a rotor diameter of 170–180 m, which matches well with the optimal rotor diameter of 170 m found in the LCOH optimization previously discussed. The authors expect that these results may shift under different configurations that could include battery storage, solar panels, or a grid connection.

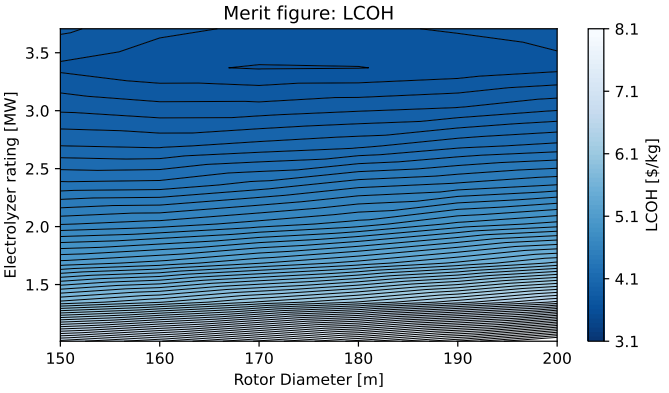

Fig. 5 How LCOH varies as the rotor diameter of the wind turbine and the electrolyzer are varied, showing a minimal LCOH when the wind turbine and electrolyzer ratings are approximately 3.4 MW and the rotor diameter is around 170 m.

4 Conclusion

This paper presented a framework for designing wind turbines for hydrogen production, using the LCOH as an objective as opposed to the more traditional LCOE metric. Results from an initial onshore case study for the Texas Gulf Coast region show that significant reductions in the cost of hydrogen can be achieved with these hydrogen-focused wind turbine designs when compared to an onshore reference wind turbine that was designed by minimizing cost of energy. Specifically, a reduction of 12.7% in LCOH was found for this single turbine case study compared to the baseline onshore wind turbine optimized for LCOE. Furthermore, a 1.5% reduction in LCOH was found compared to an LCOE optimized turbine for the specific case study site. Also, a ratio of capacity of wind turbine to electrolyzer of 1:1 was found to be optimal in this wind-hydrogen only system.

The reduction in cost is believed to be due to more consistent power production from the turbines as the optimizer drove the design to larger rotor diameters, enabling turbines to operate at rated power more often. This operation then results in a more consistent power signal to the electrolyzers, giving a higher production of hydrogen. This increase in hydrogen production offsets the increase in cost of a larger rotor diameter.

Future work includes plant-level optimization and analysis to determine the extent of cost reductions that can be achieved with hydrogen-optimized wind turbines. Also, other renewable energy sources and storage technologies could impact the optimal wind turbine design; therefore, optimization studies

This report is available at no cost from the National Renewable Energy Laboratory at www.nrel.gov/publications.

including solar panels and battery storage would be of particular interest. Additionally, it is unpractical to design a specific wind turbine for each site where you would want to produce green hydrogen. Thus, regional analysis to identify an average wind turbine design optimized for minimal LCOH based on the wind conditions for each region could be a more practical approach. Lastly, applying this same framework to offshore wind plants could reveal opportunity in low-wind areas that have been less of a priority to develop for wind energy.

5 Acknowledgements

The authors would like to acknowledge GE Vernova and Nel Hydrogen for their advisement and contributions to the research. This work was authored in part by the National Renewable Energy Laboratory, operated by Alliance for Sustainable Energy, LLC, for the U.S. Department of Energy (DOE) under Contract No. DE-AC36-08GO28308. Funding provided by U.S. Department of Energy Office of Energy Efficiency and Renewable Energy Hydrogen and Fuel Cell Technologies Office. The views expressed in the article do not necessarily represent the views of DOE or the U.S. Government. The U.S. Government retains and the publisher, by accepting the article for publication, acknowledges that the U.S. Government retains a nonexclusive, paid-up, irrevocable, worldwide license to publish or reproduce the published form of this work, or allow others to do so, for U.S. Government purposes.

6 References

[1] Hydrogen Council, 'Path to hydrogen competitiveness: A cost perspective' (Hydrogen Council, 2020), pp. 1–88

[2] Clark, C.E., Barker, A., Brunik, K., et al: 'Opportunities for green hydrogen production with land-based wind in the United States', Energy Conversion and Management, 2023, 296, pp. 117595

[3] 'Hydrogen and Fuel Cell Technology Office - Hydrogen shot', https://www.energy.gov/eere/fuelcells/hydrogen-shot, accessed 15 April 2024

[4] 'European Commission: The European Green Deal', https://commission.europa.eu/strategy-and-policy/priorities-2019-2024/european-green-deal_en, accessed 15 April 2024

[5] Mehta, M., Zaaijer, M., von Terzi, D.: 'Optimum Turbine Design for Hydrogen Production from Offshore Wind', Journal of Physics: Conference Series, 2022, 2265, (4), pp. 042061

[6] Dykes, K.: 'Optimization of Wind Farm Design for Objectives Beyond LCOE', Journal of Physics: Conference Series, 2020, 1618, (4), pp. 042039

[7] Weiß, A., Siebel, A., Bernt, M., et al: 'Impact of Intermittent Operation on Lifetime and Performance of a PEM Water Electrolyzer', Journal of The Electrochemical Society, 2019, 166, (8), pp. 487–497

[8] Shaun, A.M., Stariha, S., Borup, R.L.: 'Electrolyzer Durability at Low Catalyst Loading and with Dynamic Operation', Journal of The Electrochemical Society, 2019, 166, (15), pp. 1164–1172

[9] Bortolotti, P., Tarres, H.C., Dykes, K.L., et al, 'IEA Wind TCP Task 37: Systems Engineering in Wind Energy-WP2.1 Reference Wind Turbines' (NREL, 2019), pp. 1–138

[10] NREL, 'Wind-Plant Integrated System Design and Engineering Model (WISDEM®)', https://github.com/WISDEM/WISDEM, Version: f893264, [code], accessed 15 April 2024

[11] Gray, J.S., Hwang, J.T., Martins, J.R.R.A, et al: 'OpenMDAO: An Open-Source Framework for Multidisciplinary Design, Analysis, and Optimization', Structural and Multidisciplinary Optimization, 2019, 59, (4), pp. 1075–1104

[12] NREL, 'Electrolyzer', https://github.com/NREL/electrolyzer, Version: 55d307b, [code], accessed 15 April 2024

[13] Gill, P.E., Murray, W., Saunders, M.A.: 'SNOPT: An SQP algorithm for large-scale constrained optimization', SIAM review, 2005, 47, (1), pp. 99–131

[14] Yigit, T., Selamet, O.F.: 'Mathematical modeling and dynamic Simulink simulation of high-pressure PEM electrolyzer system', International Journal of Hydrogen Energy, 2016, 41, (32), pp. 13907–13914

[15] Ruuskanen, V., Koponen, J., Huoman, K., et al: 'PEM water electrolyzer model for a power-hardware-in-loop simulator', International Journal of Hydrogen Energy, 2017, 42, (16), pp. 10775–10784

[16] Yodwong, B., Guilbert, D., Phattanasak, M., et al: 'Faraday's Efficiency Modeling of a Proton Exchange Membrane Electrolyzer Based on Experimental Data', Energies, 2020, 13, (18), pp. 4792

[17] Tully, Z., Starke, G., Johnson, K., et al: 'n Investigation of Heuristic Control Strategies for Multi-Electrolyzer Wind-Hydrogen Systems Considering Degradation'. 2023 IEEE Conference on Control Tech- nology and Applications (CCTA), August 2023, pp. 817–822

[18] Singlitico, A., Østergaard, J., Chatzivasileiadi, S.: 'Onshore, offshore or in-turbine electrolysis? Techno-economic overview of alternative integration designs for green hydrogen production into Offshore Wind Power Hubs', Renewable and Sustainable Energy Transition, 2021, 1, pp. 100005

[19] Hunter, C.A., Penev, M.M., Reznicek, E.P, et al: 'Techno-economic analysis of long-duration energy storage and flexible power generation technologies to support high-variable renewable energy grids', 2021, Joule, 5, (8), pp. 2077–2101

[20] Mowers, M., Mai, T.: 'An evaluation of electricity system technology competitiveness metrics: The case for profitability', The Electricity Journal, 2021, 34, (4), pp. 106931

[21] Burton, T.: 'Chapter A12.1', in: 'Wind Energy Handbook' (John Wiley & Sons, Inc., 2021, 3rd edn.)

[22] NREL, 'Wind Integration National Dataset (WIND) Toolkit', https://www.nrel.gov/grid/wind-toolkit.html, [dataset], accessed 15 May 2023

This report is available at no cost from the National Renewable Energy Laboratory at www.nrel.gov/publications.